Available online at www.sciencedirect.com

ScienceDirect

www.elsevier.com/locate/brainres

Brain Research

Research Report

A novel method for quantifying similarities between oscillatory neural responses in wavelet time–frequency power profiles

Takaaki Sato[a,*], Riichi Kajiwara[b], Ichiro Takashima[c], Toshio Iijima[d]

[a]Biomedical Research Institute, National Institute of Advanced Industrial Science and Technology (AIST), Ikeda 563–8577, Japan
[b]School of Science and Technology, Meiji University, Kawasaki 214–8571, Japan
[c]Human Technology Research Institute, AIST, Tsukuba 305–8568, Japan
[d]Graduate School of Life Sciences, Tohoku University, Sendai 980–8577, Japan

ARTICLE INFO

Article history:
Accepted 29 January 2016
Available online 6 February 2016

Keywords:
Cross-correlation analysis
Oscillatory local field potentials
Wavelet transformation
Sensory information processing
Odor representation
Isolated whole brain

ABSTRACT

Quantifying similarities and differences between neural response patterns is an important step in understanding neural coding in sensory systems. It is difficult, however, to compare the degree of similarity among transient oscillatory responses. We developed a novel method of wavelet correlation analysis for quantifying similarity between transient oscillatory responses, and tested the method with olfactory cortical responses. In the anterior piriform cortex (aPC), the largest area of the primary olfactory cortex, odors induce inhibitory activities followed by transient oscillatory local field potentials (osci-LFPs). Qualitatively, the resulting time courses of osci-LFPs for identical odors were modestly different. We then compared several methods for quantifying the similarity between osci-LFPs for identical or different odors. Using fast Fourier transform band-pass filters, a conventional method demonstrated high correlations of the 0–2 Hz components for both identical and different odors. None of the conventional methods tested demonstrated a clear correlation between osci-LFPs. However, wavelet correlation analysis resolved a stimulus dependency of 2–45 Hz osci-LFPs in the aPC output layer, and produced experience-dependent high correlations in the input layer between some of the identical or different odors. These results suggest that redundancy in the neural representation of sensory information may change in the aPC. This wavelet correlation analysis may be useful for quantifying the similarities of transient oscillatory neural responses.

Abbreviations: aPC, anterior piriform cortex; aPCvr, ventro-rostral region of the aPC; EOG, electro-olfactogram; FFT, fast Fourier transform; LFP, local field potential; LOT, lateral olfactory tract; OR, olfactory receptor; osci-LFP, oscillatory local field potential; PC, piriform cortex

*Corresponding author. Fax: +81 72 751 8370.
E-mail address: taka-sato@aist.go.jp (T. Sato).

http://dx.doi.org/10.1016/j.brainres.2016.01.054

1. Introduction

In the sensory system, the neural representation of a given stimulant is coded by activation of a specific subset of receptors overlapping to varying degrees with those of other stimulants. This overlap creates a degree of redundancy in these neural representations. Because such redundancy in neural representations is likely to change at different stages of sensory information processing, quantifying the similarities and differences between neural response patterns in sensory neurons and higher brain centers is an important step in understanding sensory neural coding. Sensory systems generate oscillatory activities between related cortical regions and the thalamus, which acts (except in the olfactory system) to gate sensory input to the cortex and provide feedback from cortical pyramidal neurons. While stationary oscillatory activity is relatively simple to compare, the degree of similarity or difference in transient oscillatory responses is significantly more difficult to analyze.

Among the mammalian sensory systems, the olfactory system has one of the most highly diverse repertoires of receptors (olfactory receptors; ORs), which makes it ideal for quantifying various similarities and differences between oscillatory responses. In olfaction, transient oscillatory local field potentials (osci-LFPs) are induced in the olfactory bulb (Adrian, 1950; Bressler and Freeman, 1980; Chapman et al., 1998; Chabaud et al., 2000; Lam et al., 2000) and in the anterior piriform cortex (aPC) (Bressler and Freeman, 1980; Ketchum and Haberly, 1993; de Curtis et al., 1994; Chapman et al., 1998; Chabaud et al., 2000; Ishikawa et al., 2007). In this pathway (Ishikawa et al., 2007), as well as in the other sensory thalamocortical circuit (Bruno, 2011), strong feed-forward inhibition is present. Possible integration of OR signals in the aPC (Desmaisons et al., 1999; Kashiwadani et al., 1999; Stettler and Axel, 2009) appears to be mediated via input synchronization by the above feed-forward inhibition (Ishikawa et al., 2007; Sato et al., 2008, 2015) transferred through an OR-specific pathway (Mombaerts et al., 1996; Serizawa et al., 2006). This signal integration, when occurring between different but overlapping ORs, could markedly change redundancy in the neural representations. Odorants activated different overlapping subsets of ~1000 murine ORs (Buck and Axel, 1991; Malnic et al., 1999, 2004; Zhang and Firestein, 2002), whose signals could be integrated in the aPC pyramidal cells. For example, ORs for carvones are estimated to include 70 types, with >80% overlap between carvone enantiomers (Hamana et al., 2003). The most sensitive dorsal ORs are critical for the supersensitive discrimination of the enantiomers (Sato et al., 2015), and despite the high degree of overlap, mice can easily discriminate between the carvone enantiomers even at high concentrations.

Thus far, there are no published methods for quantifying the similarity of aPC oscillatory responses, despite the need to understand the mechanism and relationships underlying the change in redundancy of neural representations in the aPC. In an analog of the mammalian olfactory cortex, the insect mushroom body, sliding cross-correlations between unit responses and LFPs were analyzed to attempt to identify response synchrony (Stopfer et al., 1997; Perez-Orive et al., 2002), whereas one study analyzed the wavelet coefficients for spike trains in the insect anntenal lobe (Capurro, et al., 2014).

Here, we compared several methods for quantifying the similarity of aPC osci-LFPs between identical or different odors. We first tried conventional methods, including cross-correlations between frequency band components generated through fast Fourier transform (FFT) band-pass filters. We then tried a novel method of wavelet correlation analysis, using sets of logarithmic ratios of cross-correlations to auto-correlations at representative frequencies, and compared the data collected using conventional versus the wavelet methods.

2. Results

2.1. *Odor-evoked osci-LFPs in the aPC were not strictly phase-locked to the stimulus onset and were not stationary over the time window of interest*

Odor-evoked osci-LFPs were recorded in an *ex vivo* isolated whole brain with attached nose preparation (Ishikawa et al., 2007; Sato et al., 2008). We first examined the reproducibility of odor-evoked osci-LFPs in layer I of the aPC. Through repeated 1-s presentation of identical odors, osci-LFPs showed similar but somewhat distinct temporal profiles (Supplementary Fig. S1). Moreover, a pair of quite different odors (Lav and mc468) evoked dissimilar osci-LFPs. Osci-LFPs began during the odor presentation, before the peak of the receptor potential: electro-olfactogram (EOG) response (the lowest trace in Supplementary Fig. S1). To calculate the correlation coefficients of the temporal profiles of these osci-LFPs, we employed a 2.5-s time window that was comprised of the 1-s odor presentation and the following 1.5 s.

Correlations of the temporal profiles of osci-LFPs were not homogeneously high between identical odors (Supplementary Fig. S2A). In 3 of the 28 Lav pairs, and the only 0.1-Lav pair, the correlations were relatively high (0.7–0.74). The remaining 25 Lav pairs demonstrated intermediate correlations of 0.47–0.69, and the mc468 pair demonstrated a low value of 0.29. These low correlations between osci-LFPs for identical odors may have been caused by differences in the oscillatory phase angles. Superimposed traces revealed that oscillatory components demonstrated independent fluctuations in phase angles and oscillatory powers including a few synchronous cycles even between identical odors (Supplementary Fig. S3). Some of the phase-matching points are indicated in Supplementary Fig. S3 by daggers. These results indicate that odor-evoked osci-LFPs in the aPC are not strictly phase-locked to the stimulus onset, and are not stationary over the time window of interest. That is, these properties prevented traditionally derived correlations of the temporal profiles from demonstrating the stimulus dependency of the osci-LFPs. Next, to identify the origin of the high correlations that were obtained between some of cases, we analyzed the contribution of different frequency components.

2.2. *The spurious high correlations originated in the low frequency band*

By using FFT band-pass filters, cross-correlations were compared between frequency band components of odor-evoked osci-LFPs of the 2.5-s time window. All 28 Lav pairs and one 0.1-Lav pair demonstrated high correlations (>0.77) for the 0–2-Hz component of osci-LFPs (Supplementary Fig. S2B), whereas all pairs showed low correlations (<0.4) for the 2–45 Hz components (Supplementary Fig. S2C). These results indicate that the high correlations between the osci-LFPs are primarily attributable to similarities in the temporal profiles of the 0–2-Hz components (Supplementary Fig. S4). In addition, the 0–2-Hz component of the 2nd mc468 demonstrated high correlations (0.66–0.81) with 5 of 6 Lav responses, whereas the 1st mc468 response showed low correlation (0.27–0.54) with all 6 Lav responses. These results indicate that conventional correlations between the 0–45-Hz or 2–45-Hz temporal profiles are not suitable for quantifying similarity between the osci-LFPs. Because of the spurious high correlations in the low frequency band, all 0–2-Hz component were removed prior to phase-tolerant analysis of the 2–45-Hz components of the osci-LFPs.

2.3. *FFT analysis could not resolve stimulus dependency of osci-LFPs in the aPC*

FFT power spectra of the odor-evoked osci-LFPs were not reproducible among identical odors (Supplementary Fig. S5). As the final analysis in conventional methods, the FFT spectra for sequential sets of 0.4-s (400 points), 0.8-s (800 points), or 1.0-s (1000 points) time windows were compared between identical odors. These trials also failed to demonstrate the stimulus dependency of the osci-LFPs (data not shown). The disappearance of the stimulus characteristics in FFT low time-resolution would cause the low correlations between the osci-LFPs. Thus, the above conventional methods for quantifying the similarity of odor-evoked osci-LFPs were deficient in time–frequency power resolution and in tolerance of trial-by-trial oscillatory phase differences. To address these weaknesses, we tested a novel correlation analysis of wavelet profiles.

2.4. *Wavelet correlation analysis of time–frequency power profiles resolve stimulus dependency of odor-evoked osci-LFPs*

Fig. 1 shows the procedure for the wavelet transformation and its conversion to a data array for wavelet correlation analysis (see the Experimental Procedures). Wavelet profiles of identical odors resembled each other more than they resembled those of different odors (Fig. 2). To quantify the wavelet similarities of odor-evoked osci-LFPs in transient changes in oscillations, we employed the logarithmic ratios of cross-/auto-correlations of a time window of interest (time lag=0) (Fig. 1C), and calculated correlation coefficients of the columnar arrays of the logarithmic ratios of pairwise wavelet profiles at 9 representative frequencies as a wavelet correlation matrix. Fig. 3 presents the array data of the logarithmic ratios of wavelet cross-/auto-correlations of a 2.5-s time window between 13 odor-evoked osci-LFPs. The logarithmic ratios, displayed as the lengths of the bars for the cross-/auto-correlations of wavelet profiles at the 9 frequencies, reflected differences between the pair of osci-LFPs in such a way that the values of +1, 0, and −1 represent cross-correlations that are 10-fold, equal to, and one-tenth of the auto-correlation at the respective frequencies.

The wavelet correlation matrix enabled us to demonstrate higher correlations between the osci-LFPs for identical odors than between those of different odors. In contrast to the low correlations (<0.4) between the 2–45-Hz components using conventional methods (Supplementary Fig. S2C), the wavelet

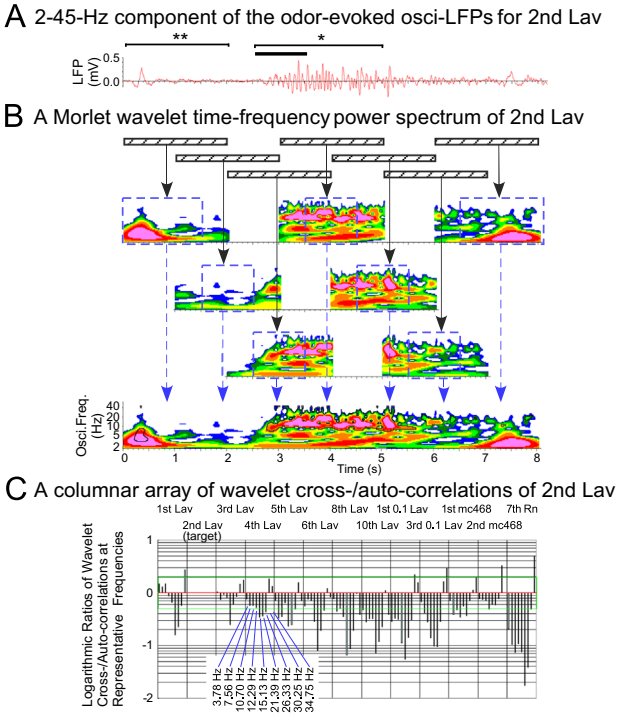

Fig. 1 – Wavelet transformation of an oscillatory response and its wavelet cross-correlation profile. A: The 2–45-Hz component of odor-evoked osci-LFP for the second presentation of Lav (2nd Lav) to the nose of an isolated brain. The horizontal bold bar indicates the duration of odor presentation. B: A Morlet wavelet time–frequency power spectrum of an odor-evoked osci-LFP. Seven sets of 2048-point wavelet transformations of the osci-LFPs were then calculated. The wavelet power in the regions within the black lines was significantly higher ($P<0.0001$, χ^2-test) when compared to the average wavelet power of the pre-stimulus period (10–2057 ms, marked with the double asterisks in (A) across all recordings from the same brain. C: A columnar array of wavelet cross-/auto-correlations of the second Lav-evoked response. Sets of logarithmic ratios of cross-correlation to auto-correlation between wavelet pairs of the 2nd Lav-evoked response (target) and one of the responses for the time window of interest (2.5 s, marked with the asterisk in (A)) at 9 representative frequencies were serially concatenated into a data array. This logarithmic cross-correlation profile likely represents similarities in the time–frequency power profiles between responses. Wavelet correlations were calculated as correlation coefficients between the pairwise columnar array data.

correlation matrix demonstrated high correlations (>0.76) between osci-LFPs for the identical odors along the diagonal line in the matrix (Fig. 4A). These results indicate that the time–frequency power profiles of osci-LFPs in layer I of the aPC partially resemble each other in a stimulus-dependent manner. In addition, rearranging the correlation matrix to match the order of odor presentation generated a moderate cluster of high correlations, even between different odors as long as the condition of being within a few sequential presentations was met (Fig. 4B, diagonal area between the dashed lines). This feature suggests that a subsequently applied odor evoked osci-LFPs in layer I of the aPC that resembled those evoked by the previous odor (i.e., experience-dependently). Notably, such a clustering of high correlations was not found in the rearranged correlations for the 0–2 Hz component (Supplementary Fig. S2D).

In addition, wavelet transformation enabled visualization of the characteristic features of odor-evoked osci-LFPs in

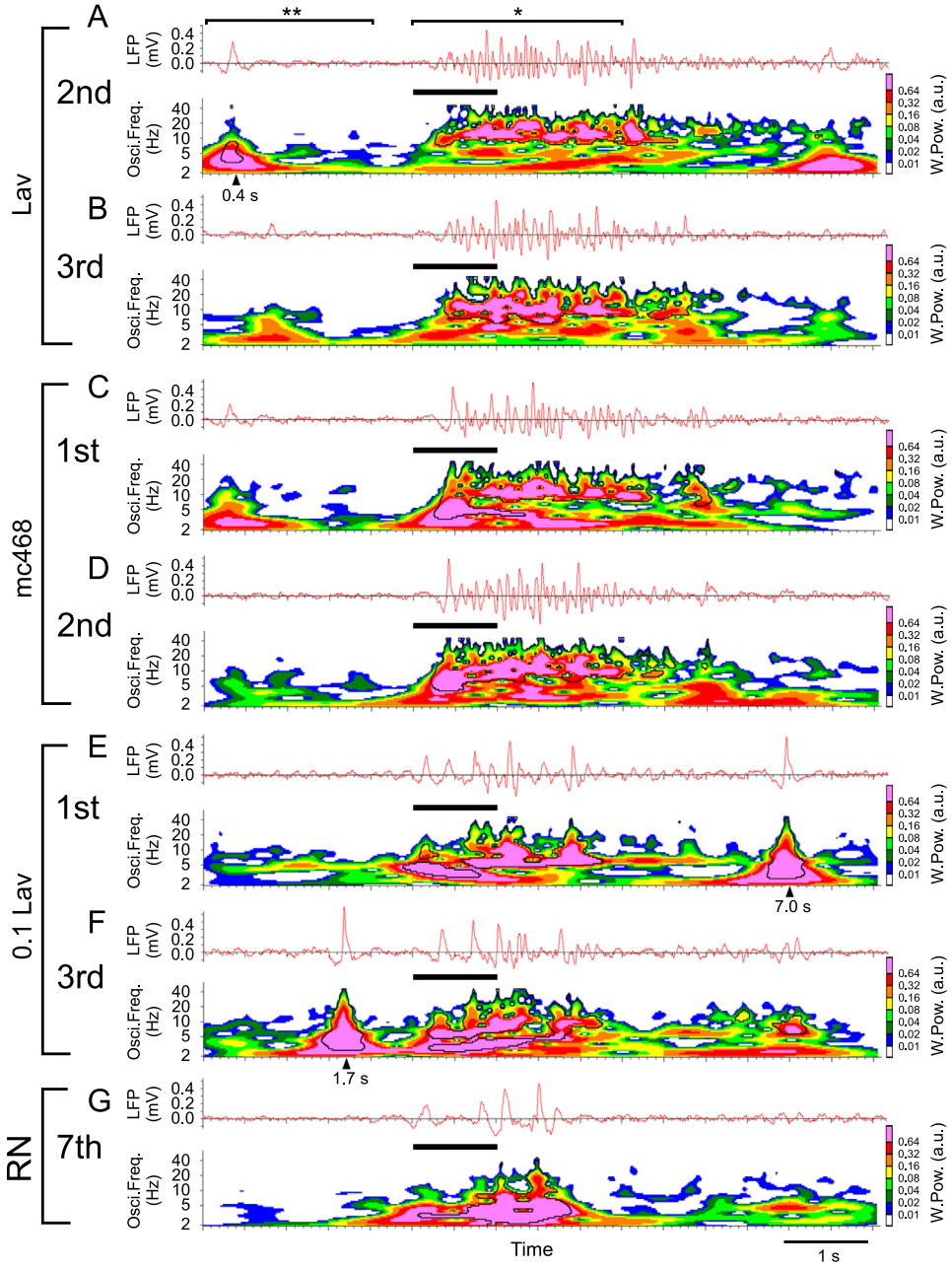

Fig. 2 – Wavelet profiles of the odor-evoked osci-LFPs in layer I of the aPC. The 2–45 Hz components (upper traces) of the odor-evoked osci-LFPs (shown in Supplementary Fig. S1) were transformed into time–frequency power profiles (lower traces). The wavelet profiles for identical odors resembled, while they were dissimilar to those of different odors. Random spontaneous activity was observed. Correlation analysis was performed for a 2.5-s time window (marked by the asterisk). Compared to the pre-stimulus activity (indicated by the double asterisks), the profiles inside the black lines correspond to significant increases in wavelet power ($P<0.0001$, χ^2-test). The 8 orders of wavelet power in the binary scale are represented by the different colors (<0.01, white; <0.02, blue; <0.04, green; <0.08, yellow-green; <0.16, yellow; <0.32, orange; <0.64, red; ≥0.64, pink).

layer I of the aPC, especially the scattering of transient reductions in oscillatory power at different frequencies. Many small spots of reduced activity were relatively concentrated at frequencies just above 10 Hz. Furthermore, the wavelet power at ~40 Hz was quite small, yet was still significantly greater than pre-stimulus activity (Fig. 2, $P<0.0001$, χ^2-test; within the black lines). In contrast, the initial phase of the wavelets for mc468-evoked osci-LFPs had distinct characteristics: During the initial phase, power at all frequencies was greater than that of the Lav-evoked response (Figs. 2A and B); and this was followed by a transient decrease in the low-frequency band for ~0.6 s (Figs. 2C and D). The FFT power spectra also demonstrated that the dominant components of odor-evoked osci-LFPs resided in the 6–25 Hz frequency

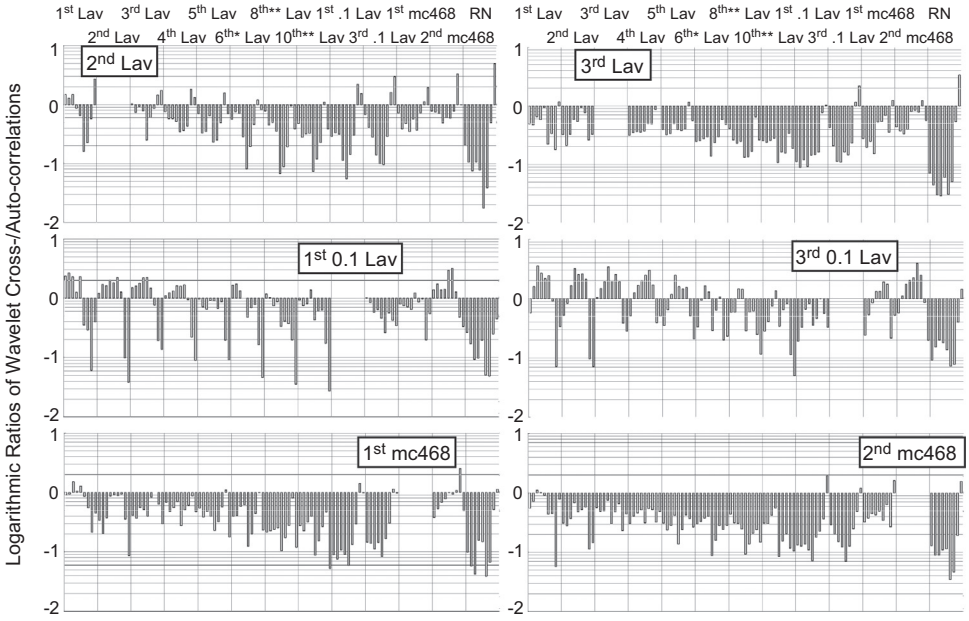

Fig. 3 – Identical stimuli produced similar wavelet cross-correlation profiles of the osci-LFPs. The logarithmic ratios of wavelet cross-correlations to auto-correlations for each pair-wise combination between 13 odor-evoked osci-LFPs was calculated for the 2.5-s time window (shown in Fig. 2) at each representative frequency. The degree of difference between the time courses of the wavelet powers increased, as depicted by increasing length of the bar. Wavelet correlations were calculated as correlation coefficients among these columnar data arrays (Figs. 4A, and B).

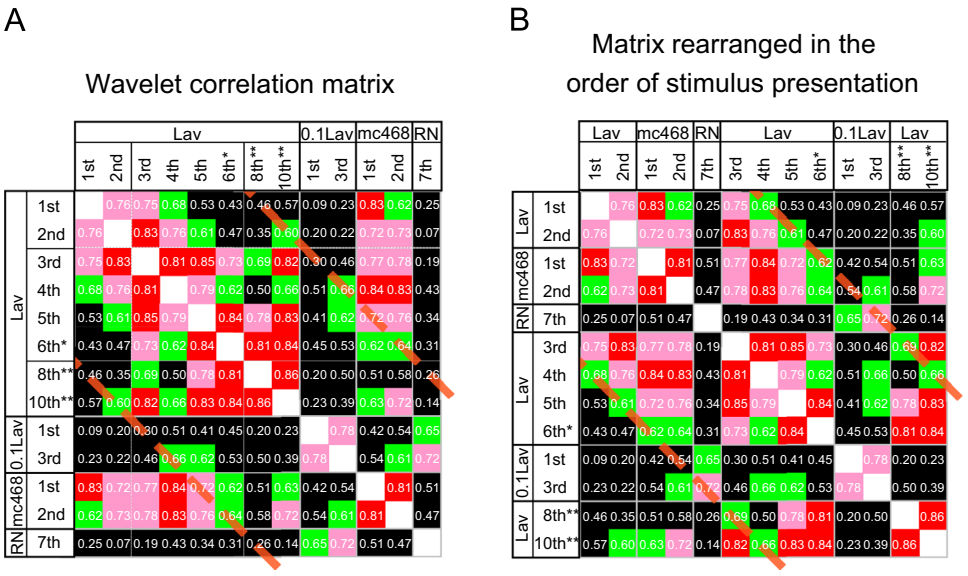

Fig. 4 – Wavelet correlation matrices among odor-evoked osci-LFPs in layer I of the aPC. A: Wavelet correlation matrix of the 2–45-Hz components of the osci-LFPs (shown in Fig. 2). The correlations for some of the identical odors were increased again. B: Matrix in A rearranged in the order of stimulus presentation. The high correlations approached the diagonal line (between the dashed lines). The amplitude of the cross-correlation is represented by the different colors: black, <0.60; green, 0.60–0.69; pink, 0.70–0.79; red, 0.80–0.89; orange, 0.90–0.99; and white, 1.00.

range, unlike the dominant components of RN-evoked responses, which were in the 2–6 Hz frequency range (Supplementary Fig. S5). Notably, in *in vivo* recordings of responses in the aPC, 0–15-Hz components formed at least 60% of the power of the total oscillatory activity, but these components could not be used because of their possible origin in the respiratory system or in endogenous θ oscillations (Lam et al., 2000). Using the isolated, nose-attached whole brain (i.e., no respiration), odorants evoked olfactory-related >6 Hz osci-LFPs in the aPC.

2.5. *Wavelet correlation analysis of odor representation in the dorsal aPC*

Oscillatory activity in layer I of the aPC originates from afferent fibers, association fibers, and postsynaptic inhibitory feedback input, whereas the activity in layer III primarily originates from the output signals of pyramidal cells that are the principal neurons in the aPC. In a previous study, current source density analysis of odor-evoked osci-LFPs indicated that association input was an important contributor to osci-LFPs in layer Ib (Ishikawa et al., 2007). Here, we examined the differences in the odor representations between these input and output layers (layers I and III, respectively). The wavelet correlation matrix of simultaneously recorded, odor-evoked osci-LFPs was compared between layer I of the centromedial site and layer I or III of the caudocentral site, a distance of approximately 1.5-mm across the dorsal aPC (Fig. 5, Supplementary Fig. S6, S7; also see Fig. 5 in Sato et al., 2008).

The initial surface positive LFPs of the odor-evoked responses were reduced in layer III of the aPC relative to those in layer I of the aPC (Fig. 5, Supplementary Fig. S6). Notably, the polarity of the LFPs reverses between layers I and III in the dorsal aPC (Ishikawa et al., 2007). In layer III, components above 10 Hz remained prominent whereas the <8-Hz components decreased relative to those in layer I (Supplementary Fig. S6). Wavelet cross-correlation profiles differed slightly between layers I and III (Supplementary Fig. S7). However, as seen in Fig. 6C, the Lav domain of the wavelet correlation matrix (broken yellow square) in layer III was homogeneously filled with high correlations, except for the 9th Lav. On the other hand, that of layer I was filled with more heterogeneous values (Fig. 6A). Other identical odor domains were similarly filled with high correlations in both layers I and III. In addition, the correlations between different single-component odors (Lina and mc4, in the broken blue squares), decreased to <0.6 in layer III (Fig. 6C), whereas over half of the correlations in the same domain in layer I were greater than 0.6 (Fig. 6A). Notably, the experience-dependent response similarity (see Section 2.4) was also observed for some of the odors in layer I of the aPC (a cluster of high correlations between the dashed lines in Fig. 6B vs. 6A), but was not clearly observed in layer III (Fig. 6D vs. 6C). These results suggest that the oscillatory output of dorsal aPC pyramidal cells represents odor identity through a population-coding system. This means that sensory information redundancy of neural representation may change from experience to stimulus dependency in the aPC. Based on the above correlations, this novel wavelet correlation analysis was useful for quantifying similarities of oscillatory cortical responses, even transient responses, and for examining neural coding processes.

2.6. *Sensitivity of wavelet correlation analysis to changes in oscillatory components*

It would be useful to understand how sensitive the wavelet correlation analysis to differences in oscillatory response profiles, so we compared wavelet correlations with 0.2-fold to 2.0-fold amplification (0.2-fold steps) at 1–8 frequency bands (Fig. 7, Supplementary Figs. S8, S9). Power amplification of the wavelet profiles caused a factor-dependent change in wavelet correlations. The 0.2-fold power amplification at only 1–2 of the 9 frequencies resulted in greater decreases in correlations (0.4–0.7) than power amplification at 8 frequencies (number/9 given in parentheses on the Y-axis). In the case of 0.2-fold power amplification, the greatest decrease was observed at 8–13 Hz, whereas the smallest decrease was at 4–8 Hz. Interestingly, these effects were inverted in the case of 2.0-fold power amplification. This result suggests that in these odor-evoked osci-LFPs, the 8–13-Hz component contributes to the correlation coefficients more than the 4–8-Hz component. It is also notable that components of the 4 frequency bands (2–4 Hz, 13–20 Hz, 20–30 Hz, 30–45 Hz) modestly contribute to the wavelet correlations. Because the number of representative frequencies for 2-fold wavelet power modification increased to more than 4, the extent of

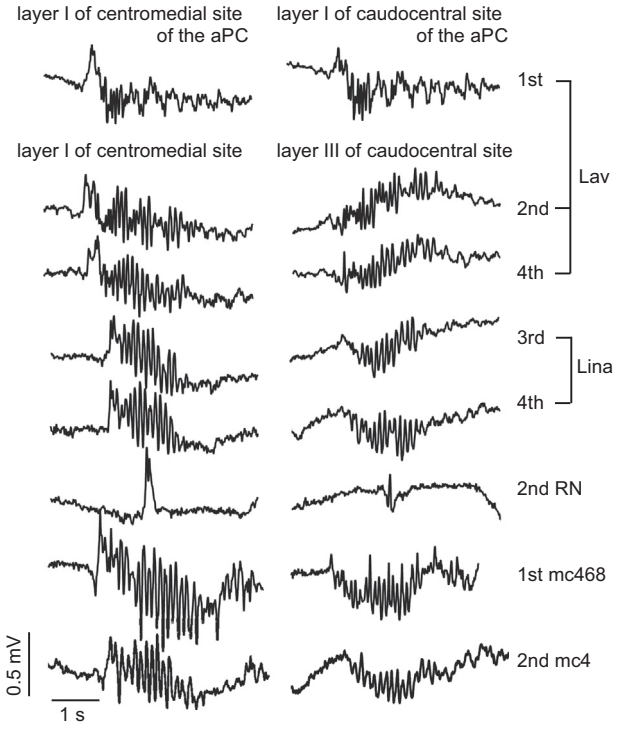

Fig. 5 – Odor-evoked osci-LFPs differed between the input and output layers of the aPC. Of 21 pairs of osci-LFPs that were simultaneously recorded in layer I (mainly input signals to pyramidal cells) of the centromedial site and layer I or layer III (mainly output signals from pyramidal cells) of the caudocentral site of the dorsal aPC, 8 representative pairs are described here. The two recording sites were horizontally ~1.5-mm apart. In the output layer, the initial surface positive LFP was reduced in the low frequency band, compared to the more prominent 10 Hz frequency of both the input and output layers (see Supplementary Fig. S6).

change in the wavelet correlations was reduced. This analysis could be useful for estimating the relative contributions of oscillatory components to wavelet correlations.

3. Discussion

3.1. *A novel method of wavelet correlation analysis in the context of wavelet transformations*

A novel method of wavelet correlation analysis, using sets of logarithmic ratios of cross-correlations to auto-correlations at representative frequencies, resolved the stimulus dependency of odor-evoked osci-LFPs in layer III of the aPC and the difference in responses before and after OR signal integration between layers I and III. These results suggest that sensory information redundancy changes in aPC pyramidal cells, in this case, by reduction of an experience-dependent correlation between odor responses in the output layer of the aPC pyramidal cells. It is likely that the reason the wavelet correlation analysis was the only method able to resolve the stimulus dependency of transient oscillatory responses is its excellent sensitivity to subtle time variations that frequently escape detection by other approaches. Indeed,

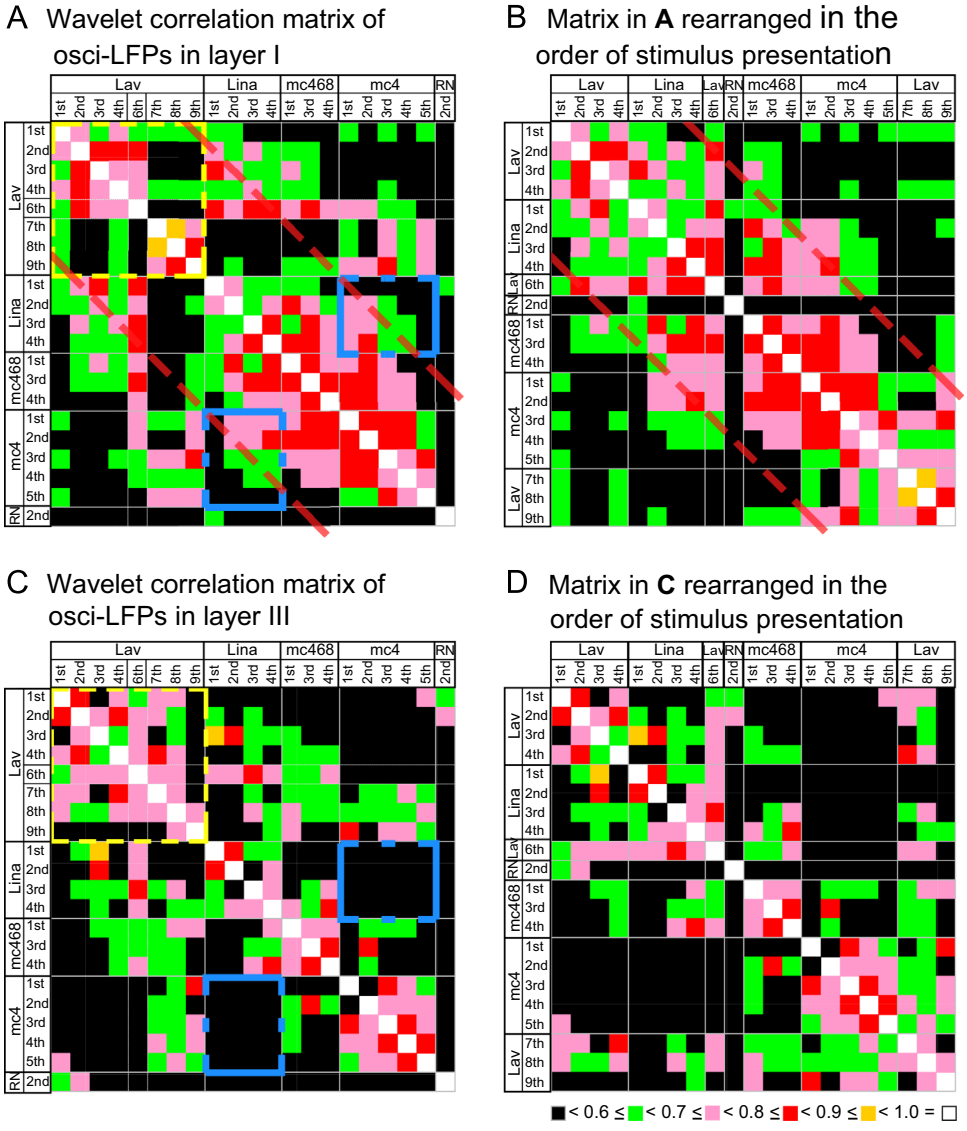

Fig. 6 – Wavelet correlation matrices of osci-LFPs differed between the input and output layers of the aPC. A: The wavelet correlation matrix of osci-LFPs in layer I (mainly input to the aPC pyramidal cells) for the 2.2-s time window (shown in Supplementary Fig. S6). B: The matrix in (A) rearranged in the order of stimulus presentation. As also shown in Fig. 4B, high correlations approached the diagonal line. C: The wavelet correlation matrix of osci-LFPs in layer III (mainly output from the aPC pyramidal cells) of the 2.2-s time window. The domains of identical odors, especially for Lav (broken yellow square), were mostly occupied with high correlations in the output layer of the aPC, but not in the input layer. In addition, correlations between the single component odors Lina and mc4 (broken blue square) decreased to <0.6 in the output layer, but some were high in the input layer. D: The matrix in C rearranged in the order of stimulus presentation. The colors that represent the magnitude of the correlations are the same as those described in Supplementary Fig. S2.

the wavelet transform was used elsewhere to visualize fine differences in oscillatory responses in time–frequency power profiles (Dorries and Kauer, 2000; Capurro et al., 2014). In this study, we further combined the wavelet transform and ratio profiling of cross-/auto-correlations at several representative frequencies. This particular time–frequency power analysis improved both the tolerance to trial-by-trial oscillatory phase differences (Supplementary Fig. S2C, Fig 4A, Supplementary Fig. S5) and the time resolution (Fig. 2).

3.2. *Implications for the role of inhibition in odor information processing in the olfactory bulb and aPC*

Generation of oscillatory activity requires both recurrent input and its synchronization by inhibitory signals. Proper odor discrimination also requires enhancing the characteristic odor representation and reducing the significant overlap in cellular responses between different odors, both of which are achieved through selective inhibition. Here, we discuss the implied relationship between inhibitory activity and odor information processing in the olfactory bulb and aPC.

Mitral cells and tufted cells that receive identical OR signals in a single glomerulus convey different aspects of odorant information to the olfactory cortex (Nagayama et al., 2004; Igarashi et al., 2012). The bulbocortical projection is partially organized with sensitivity dependence. Within this

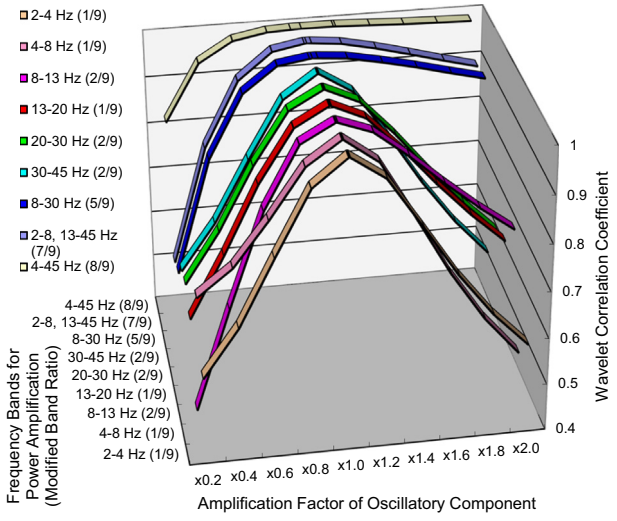

Fig. 7 – Sensitivity of wavelet correlation coefficients to changes in oscillatory components. In order to examine the effects of partial changes in wavelet power profiles on wavelet correlations, oscillatory components in several frequency bands were modified by amplification factors (0.2–2.0). In the case of 0.2-fold power amplification, the greatest decrease was observed at 8–13 Hz, whereas the smallest decrease was at 4–8 Hz. The opposite was true in the case of 2.0-fold power amplification. As the number of representative frequencies for wavelet power modification increased to more than 4, the extent of change in the wavelet correlations was reduced. Notably, high values ($>$0.9) of wavelet correlations were observed for the 2-fold power amplification at 8 out of the 9 representative frequencies.

organizational hierarchy, middle tufted cells respond to odorants with higher firing rates under weak or no inhibition than mitral cells. Optical recordings revealed that the rostral part of the aPC (aPC_R) is more sensitive to odors than the caudal part in guinea pigs (Sugai et al., 2005). This correlates anatomically with the preferential projection of tufted cells to the anterior olfactory nucleus and aPC_R in rats (Haberly and Price, 1977; Matsutani et al., 1989; Ekstrand et al., 2001). It also correlates with dense projections to targets localized to anterior areas of the olfactory cortex, including the aPCvr, but not the dorsal aPC, in mice (Igarashi et al., 2012). Miyamichi et al. demonstrated that unlike layer I GABAergic neurons, which have significant mitral cell innervation, layer II/III GABAergic neurons in the aPC receive little direct mitral cell input (Miyamichi et al., 2011). At present, it is unknown whether the feed-forward inhibition to the caudal aPC is direct (from aPCvr) or indirect (via layer-II/III GABAergic neurons).

Our analysis indicated a difference in sensory information redundancy of neural representation between layer I and layer III of the aPC. The aPC pyramidal cells integrate different OR signals that are synchronized by feed-forward, local, and feedback inhibition. The aPCvr is the signal source of the feed-forward inhibition to the pyramidal cells in the aPC (Ishikawa et al., 2007; Sato et al., 2008). The oscillatory responses in layer I (the input layer to the aPC pyramidal cells) mainly originate from the afferent fibers from the olfactory bulb mitral/tufted cells, whereas those in layer III (the output layer) primarily originate from the axons of aPC pyramidal cells. The influence of previously presented odors had been identified in the piriform cortex and orbitofrontal cortex during odor discrimination in behaving rats (Schoenbaum and Eichenbaum, 1995). In the aPC, rapid experience-induced enhancement in odorant discrimination was also observed (Wilson, 2003), in addition to odor habituation for long odor exposures (Wilson, 1998, 2000). An intrinsic network property, such as the 5 Hz or 20 Hz induced short-term depression of the afferent fiber pathway, or the short-term facilitation in the association fiber pathway (Hasselmo and Bower, 1990), may partially contribute to such experience-dependency in layer I of the aPC.

A genetic ablation of all dorsal ORs resulted in $>10^{10}$-fold reductions in enantiomer discrimination sensitivities in mice while retaining the supersensitivity to (−)-enantiomers (Sato et al., 2015). This result indicates that the most sensitive dorsal ORs play a critical role in hierarchical odor coding by contributing to mutual inhibition between elemental odors. Mutual inhibition between different odors or different elemental odors was previously examined in a mixture of rose and fox-unique TMT odors (Matsukawa et al., 2011). The rose-odor-induced decrease in cells positive for TMT odor in the aPCvr and the subsequent decrease in fear response suggested that the signals from ORs activated by the co-applied rose odor weakened the feed-forward inhibition from ORs for TMT and thus the subsequent signal integration of cognate TMT ORs. Compared to the sum of the responses to the 2 individual odors, the total number of cells positive for the mixture of TMT and rose odor in the dorsal part of the aPC also decreased, suggesting a decrease in the perceived intensity of the TMT odor (Matsukawa et al., 2011). Interestingly,

hinokitiol (woody) odor can alleviate the TMT-induced stress with no significant decrease in aPCvr activity, unlike the rose odor (Murakami et al., 2012). In contrast to these two odors, caraway odor did not alleviate the TMT-induced stress. There is also evidence of mutual inhibition in the aPC. Two-photon imaging of the odor responses in the aPC in mice revealed that 40–60% of the cells responsive to the individual octanal or α-pinene odorants did not respond to a mixture of these components (Stettler and Axel, 2009). On the other hand, mixture facilitation of odorant-evoked responses in the aPC has also been reported (Chapman et al., 1998; Yoshida and Mori, 2007).

In insects, the importance of synchronization via inhibition for similar odor discrimination is well-documented (Stopfer et al., 1997; Assisi et al., 2007). Moreover, aPC pyramidal cells send projections back to the olfactory bulb and anterior olfactory nucleus (Haberly, 2001), in addition to their excitatory innervation of the inhibitory granule cells (Dennis and Kerr, 1976; Nakashima et al., 1978). The hierarchical odor-coding scheme acts to automatically enhance the characteristic elements of odor qualities by mutual inhibition, and by signal synchronization driven by signals from the most sensitive receptors. This can help to maintain constancy of odor percept over a wide range of stimuli (Sato et al., 2008, 2015). Olfactory information from the aPC is further transferred and processed in the posterior PC, the amygdaloid cortex and the entorhinal cortex (Kajiwara et al., 2007). Further analyses of neural coding in sensory neurons and higher brain centers, including those utilizing this novel wavelet correlation analysis for transient oscillatory responses, are required to more fully understand the processes in sensory neural coding.

4. Conclusions

We developed a novel wavelet correlation analysis for quantifying differences and similarities in oscillatory responses. This method revealed differences in oscillatory cortical responses between layers I and III of the aPC, the responses for which predominantly originate from the inputs and outputs of the aPC pyramidal cells, respectively. Our results suggest that sensory information redundancy in neural representations may change from an experience dependency to a stimulus dependency in the aPC pyramidal cells. This wavelet correlation analysis may be useful for quantifying similarities between oscillatory neural responses and for examining the neural coding processes not only in the olfactory cortex, but also in other sensory systems.

5. Experimental procedures

5.1. *Isolation of a guinea-pig whole brain with the nose attached, recording LFPs and odor presentations to the nose*

In order to reduce the crosstalk from non-olfactory systems, we prepared the isolated whole brains of young male Hartley guinea pigs with the nose attached, as described previously (Ishikawa et al., 2007; Sato et al., 2008). Animals were treated in accordance with Japanese Law (no. 105) and the organizational guidelines for the Care and Use of Laboratory Animals in the AIST. The electrophysiological responses were differentially recorded at 27 °C with 2 glass micropipettes (3–8 MΩ input resistance) filled with RN from the olfactory epithelium or layer I or III of the aPC of isolated whole brains. Other procedures have also been described in details in previous studies (Ishikawa et al., 2007; Sato et al., 2008).

5.2. *Data analysis using wavelet transformation*

The digital filtering of LFPs was performed using band-pass or low-pass filters in FFT analysis using the program ORIGIN (MICROCAL Software, Inc.). The similarity of odor-evoked osci-LFPs was quantified using wavelet time–frequency power profiles. The wavelet transform is like a running, windowed Fourier transform; it uses a certain window size and slides it along in time, computing the FFT at each time using only the data within the window. It is suitable for analyzing time series that contain non-stationary power at many different frequencies. The original wavelet software libraries were provided by C. Torrence and G. Compo (Torrence and Compo, 1998), and modified with respect to the following points. The 2–45 Hz bandpass-filtered LFPs were subjected to a Morlet wavelet analysis by using the following equations:

$$W_n(s) = \sum_{n'=0}^{N-1} x_{n'} \psi^* \left[\frac{(n'-n)\delta t}{s} \right] \quad (1)$$

$$\psi_0(\eta) = \pi^{-1/4} e^{i\omega_0 \eta} e^{-\eta^2/2} \quad (2)$$

$$\omega_j = \frac{\omega_0 + \sqrt{2+\omega_0^2}}{4\pi s_j} \quad (3)$$

$$s_j = s_0 2^{j\delta j} \quad (j = 0, 1, \ldots J) \quad (4)$$

$$J = \delta j^{-1} \ln \frac{N\delta t}{s_0} \quad (5)$$

where the (*) indicates the complex conjugate, $\omega_0 = 6$, $N = 2048$, $\delta t = 0.001$, $s_0 = 2\delta t$, $\delta j = 0.1$. The wavelet power spectrum, $|Wn(s)|2$, was plotted in the frequency (ω_j) range from 1.89 Hz to 42.78 Hz (Fig. 1A). Wavelet transformations of 8192 data points were performed for seven epochs of 2048 ms (2^{11} sequential points at the 1000-Hz sampling rate) with a 50% overlap (Fig. 1B). Epochs were centered every 1024 data points to the 7336th data points. The time series were padded with the actual data ($s \geq 0$) or zeros ($s < 0$) around the edge of each epoch. To combine the seven epochs of overlapping wavelets from 0 to 8191 ms, the middle 2 quarters of each partial wavelet were used to avoid frequency-dependent errors that increase at the edges of the epochs (Fig. 1B). The wavelet power in the regions within the black lines was highly significant ($P < 0.0001$, χ^2-test, Figs. 1B, 2, Supplementary Figs. S5, S6), compared to the average wavelet power of a pre-stimulus period (10–2057 ms, marked with double asterisks in Fig. 1A) across all recordings from the same preparation at each frequency.

To quantify the similarities of wavelet time–frequency power profiles of osci-LFPs between identical and different odors, we used sets of ratios of cross-correlations (time

lag=0) to auto-correlations (time lag=0) of the wavelet power profile for a time window of interest at nine representative frequencies. The nine representative frequencies were selected from the calculated wavelet frequencies over the following frequency bands: Delta (3.78 Hz; range, 2–4 Hz), theta (7.56 Hz; range, 4–8 Hz), alpha (10.7 Hz for the dominant oscillation and 12.29 Hz; range, 8–13 Hz), low beta (15.13 Hz; range, 13–20 Hz), high beta (21.39 Hz and 26.33 Hz; range, 20–30 Hz), and gamma (30.25 Hz and 34.75 Hz; range, 30–45 Hz). The cross-correlation was calculated as the sum of the products of the wavelet power for a pair comprised of the target response ($|Wt(s,fi)|$) and one of the other responses ($|Wn(s,fi)|$) at the representative frequencies (f_i) from the same isolated brain in a 2–4-s time window of interest (for example, $T1$ [ms] $\leq s \leq T2$ [ms]). The autocorrelation was similarly calculated as the nine sums of the squared wavelet power for the target response. Furthermore, to equalize the degree of increase and decrease of the response amplitude in the correlation analysis, we took the logarithms of the ratios ($R_n[f_i]$) of cross-correlations to autocorrelations at the representative frequencies (fi).

$$R_n(f_i) = \frac{\sum_{s=T1}^{T2} |W_n(s,fi)||W_t(s,fi)|}{\sum_{s=T1}^{T2} |W_t(s,fi)||W_t(s,fi)|} \quad (6)$$

All sets of the nine logarithmic ratios of cross-correlations to auto-correlations for the target response were serially concatenated into a columnar array of data in the identical order of responses (Fig. 1C). This columnar array is a form of wavelet cross-correlation profile. The wavelet correlations were calculated as correlation coefficients between these columnar arrays and employed to quantify the similarities of odor-evoked osci-LFPs in the aPC.

Authors' contributions

Conceived and designed the experiments: TI TS. Constructed the brain isolation set and recording system: IT RK TS. Performed the experiments, analyzed the data, and wrote the paper: TS.

Conflict of interests

The authors declare that there are no competing financial interests.

Acknowledgments

We would like to thank Dr. Graeme Lowe for his helpful advice on the manuscript. We are also grateful to Kiyo Murano for writing the computer software for wavelet transformation, and are grateful to Kaoru Tsukada, Yuka Mimura, and Ai Muramatsu for their technical assistance in physiological experiments. This work was supported by research funding (T.I. and T.S.) from METI, Japan; Grant-in-Aids for Scientific Research (B) #22300066 (T.S.), #18300066 (T.S.) and #15H02730 (T.S.) from the MEXT, Japan; and the Human Frontier Science Program grant n-RG19/96 (T.I.).

Appendix A. Supplementary material

Supplementary data associated with this article can be found in the online version at http://dx.doi.org/10.1016/j.brainres.2016.01.054.

REFERENCES

Adrian, E.D., 1950. The electrical activities of the mammalian olfactory bulb. Electroenceph. Clin. Neurophysiol. 2, 377–388.

Assisi, C., Stopfer, M., Laurent, G., Bazhenov, M., 2007. Adaptive regulation of sparseness by feedfoward inhibition. Nat. Neurosci. 10, 1176–1184.

Bressler, S.L., Freeman, W.G., 1980. Frequency analysis of olfactory system EEG cat, rabbit, and rat. Electroenceph. Clin. Neurophysiol. 50, 19–24.

Bruno, R.M., 2011. Synchrony in sensation. Curr. Opin. Neurobiol. 21, 701–708.

Buck, L., Axel, R., 1991. A novel multigene family may encode odorant receptors: a molecular basis for odour recognition. Cell 65, 175–187.

Capurro, A., Baroni, F., Kuebler, L.S., Kárpáti, Z., Dekker, T., Lei, H., Hansson, B.S., Pearce, T.C., Olsson, S.B., 2014. Temporal features of spike trains in the moth antennal lobe revealed by a comparative time-frequency analysis. PLoS One. 9, e84037, http://dx.doi.org/10.1371/journal.pone.0084037.

Chabaud, P., Ravel, N., Wilson, D.A., Mouly, A.M., Vigouroux, M., Farget, V., Gervais, R., 2000. Exposure to behaviourally relevant odour reveals differential characteristics in rat central olfactory pathways as studied through oscillatory activities. Chem. Senses 25, 561–573.

Chapman, C.A., Xu, Y., Haykin, S., Racine, R.J., 1998. Beta-frequency (15 – 35 Hz) electroencephalogram activities elicited by toluene and electrical stimulation in the behaving rat. Neuroscience 86, 1307–1319.

de Curtis, M., Biella, G., Forti, M., Panzica, F., 1994. Multifocal spontaneous epileptic activity induced by restricted bicuculline ejection in the piriform cortex of the isolated guinea pig brain. J. Neurophysiol. 71, 2463–2476.

Dennis, B., Kerr, D.I.B., 1976. Origins of olfactory bulb centrifugal fibers in the cat. Brain Res. 110, 593–600.

Desmaisons, D., Vincent, J.D., Lledo, P.-M., 1999. Control of action potential timing by intrinsic subthreshold oscillations in olfactory bulb output neurons. J. Neurosci. 19, 10727–10737.

Dorries, K., Kauer, J.-S., 2000. Relationships between odor-elicited oscillations in the salamander olfactory epithelium and olfactory bulb. J. Neurophys. 83, 754–765.

Ekstrand, J.J., Domroese, M.E., Johnson, D.M.G., Feig, S.L., Knodel, S.M., Behan, M., Haberly, L.B., 2001. A new subdivision of anterior piriform cortex and associated deep nucleus with novel features of interest for olfaction and epilepsy. J. Comp. Neurol. 434, 289–307.

Haberly, L.B., Price, J.L., 1977. The axonal projection patterns of the mitral and tufted cells of the olfactory bulb in the rat. Brain Res. 129, 152–157.

Haberly, L.B., 2001. Parallel-distributed processing in olfactory cortex: new insights from morphological and physiological analysis of neuronal circuitry. Chem. Senses 26, 551–576.

Hamana, H., Hirono, J., Kizumi, M., Sato, T., 2003. Sensitivity-dependent hierarchical receptor codes for odours. Chem. Senses 28, 87–104.

Hasselmo, M.E., Bower, J.M., 1990. Afferent and association fiber differences in short-term potentiation in piriform (olfactory) cortex of the rat. J. Neurophysiol. 64, 179–190.
Igarashi, K.M., Ieki, N., An, M., Yamaguchi, Y., Nagayama, S., Kobayakawa, K., Kobayakawa, R., Tanifuji, M., Sakano, H., Chen, W.R., Mori, K., 2012. Parallel mitral and tufted cell pathways route distinct odor information to different targets in the olfactory cortex. J. Neurosci. 32, 7970–7985.
Ishikawa, T., Sato, T., Shimizu, A., de Curtis, M., Kakei, T., Iijima, T., 2007. Odour-driven activity in the olfactory cortex of an in vitro isolated guinea-pig whole brain with olfactory epithelium. J. Neurophysiol. 97, 670–679.
Kajiwara, R., Tominaga, T., Takashima, I., 2007. Olfactory information converges in the amygdaloid cortex via the piriform and entorhinal cortices: observations in the guinea pig isolated whole-brain preparation. Eur. J. Neurosci. 25, 3648–3658.
Kashiwadani, H., Sasaki, Y.F., Uchida, N., Mori, K., 1999. Synchronized oscillatory discharges of mitral/tufted cells with different molecular receptive ranges in the rabbit olfactory bulb. J. Neurophysiol. 82, 1786–1792.
Ketchum, K.L., Haberly, L.B., 1993. Synaptic events that generate fast oscillations in piriform cortex. J. Neurosci. 13, 3980–3985.
Lam, Y.W., Cohen, L.B., Wachowiak, M., Zochowski, M.R., 2000. Odours elicit three different oscillations in the turtle olfactory bulb. J. Neurosci. 20, 749–762.
Malnic, B., Hirono, J., Sato, T., Buck, L., 1999. Combinatorial receptor codes for odours. Cell 96, 713–723.
Malnic, B., Godfrey, P.A., Buck, L.B., 2004. The human olfactory receptor gene family. Proc. Natl. Acad. Sci. USA 101, 2584–2589.
Matsukawa, M., Imada, M., Murakami, T., Aizawa, S., Sato, T., 2011. Rose odour can innately counteract predator odour. Brain Res. 1381, 117–123.
Matsutani, S., Senba, E., Tohyama, M., 1989. Terminal field of cholecystokinin – 8-like immunoreactive projection neurons of the rat main olfactory bulb. J. Comp. Neurol. 285, 73–82.
Miyamichi, K., Amat, F., Moussavi, F., Wang, C., Wickersham, I., Wall, N.R., Taniguchi, H., Tasic, B., Huang, Z.J., He, Z., Callaway, E.M., Horowitz, M.A., Luo, L., 2011. Cortical representations of olfactory input by trans-synaptic tracing. Nature 472, 191–196.
Mombaerts, P., Wang, F., Dulac, C., Chao, S.K., Nemes, A., Mendelsohn, M., Edmondson, J., Axel, R., 1996. Visualizing an olfactory sensory map. Cell 87, 675–686.
Murakami, T., Matsukawa, M., Katsuyama, N., Imada, M., Aizawa, S., Sato, T., 2012. Stress-related activities induced by predator odor may become indistinguishable by hinokitiol odor. Neuroreport 23, 1071–1076.
Nagayama, S., Takahashi, Y.K., Yoshihara, Y., Mori, K., 2004. Mitral and tufted cells differ in the decoding manner of odour maps in the rat olfactory bulb. J. Neurophysiol. 91, 2532–2540.
Nakashima, M., Mori, K., Takagi, S.F., 1978. Centrifugal influence on olfactory bulb activity in the rabbit. Brain Res. 154, 301–306.
Perez-Orive, J., Mazor, O., Turner, G.C., Cassenaer, S., Wilson, R.I., Laurent, G., 2002. Oscillations and sparsening of odor representations in the mushroom body. Science 297, 359–365.
Sato, T., Hirono, J., Hamana, H., Ishikawa, T., Shimizu, A., Takashima, I., Kajiwara, R., Iijima, T., 2008. Architecture of odour information processing in the olfactory system. Anat. Sci. Int. 83, 195–206.
Sato, T., Kobayakawa, R., Kobayakawa, K., Emura, M., Itohara, S., Kizumi, M., Hamana, H., Tsuboi, A., Hirono, J., 2015. Supersensitive detection and discrimination of enantiomers by dorsal olfactory receptors: evidence for hierarchical odour coding. Sci. Rep. 5, 14073.
Schoenbaum, G., Eichenbaum, H., 1995. Information coding in the rodent prefrontal cortex. I. Single-neuron activity in orbitofrontal cortex compared with that in pyriform cortex. J. Neurophysiol. 74, 733–750.
Serizawa, S., Miyamichi, K., Takeuchi, H., Yamagishi, Y., Suzuki, M., Sakano, H., 2006. A neuronal identity code for the odorant receptor-specific and activity-dependent axon sorting. Cell 127, 1057–1069.
Stettler, D.D., Axel, R., 2009. Representations of odor in the piriform cortex. Neuron 63, 854–864.
Stopfer, M., Bhagavan, S., Smith, B.H., Laurent, G., 1997. Impaired odour discrimination on desynchronization of odour-encoding neural assemblies. Nature 390, 70–74.
Sugai, T., Miyazawa, T., Fukuda, M., Yoshimura, H., Onoda, N., 2005. Odour-concentration coding in the guinea-pig piriform cortex. Neuroscience 130, 769–781.
Torrence, C., Compo, G.P., 1998. A practical guide to wavelet analysis. Bull. Am. Meterol. Soc 79, 61–78.
Wilson, D.A., 1998. Habituation of odour responses in the rat anterior piriform cortex. J. Neurophysiol. 79, 1425–1440.
Wilson, D.A., 2000. Odour specificity of habituation in the rat anterior piriform cortex. J. Neurophysiol. 83, 139–145.
Wilson, D.A., 2003. Rapid experience-induced enhancement in odorant discrimination by anterior piriform cortex neurons. J. Neurophysiol. 90, 65–72.
Yoshida, I., Mori, K., 2007. Odorant category profile selectivity of olfactory cortex. J. Neurosci. 27, 9105–9114.
Zhang, X., Firestein, S., 2002. The olfactory receptor gene superfamily of the mouse. Nat. Neurosci. 5, 124–133.